A Low Cost Magnetic-Field Based Indoor Positioning System

Valter Pasku, Alessio De Angelis, Guido De Angelis, Marco Dionigi, Antonio Moschitta, Paolo Carbone
Department of Engineering
University of Perugia
Perugia, Italy
Email: valter.pasku@studenti.unipg.it, guidodeangelis@ieee.org,
{alessio.deangelis, marco.dionigi, antonio.moschitta, paolo.carbone}@unipg.it

***Abstract*—This paper describes the operation principle and experimental results of a low cost positioning system based on low frequency magnetic fields. In particular, the system prototype is realized using low cost microcontroller based boards combined with off-the-shelf components and is tested over an area of approximately 50 m^2. Experimental results show a mean positioning error lower than 0.2 m and a maximum positioning error lower than 0.7 m.**

Keywords—indoor positioning; localization; magnetic fields; resonators.

I. INTRODUCTION

In the last 10 years, the knowledge of the position of different users has become a key factor in the development of several systems and applications. Examples are the Internet of Things (IoT) [1], Location Based Services (LBSs) [2] and Ambient Assisted Living (AAL) [3] applications. While in outdoor environments the Global Positioning System (GPS) solution is a well-established choice, in indoor environments it has a low applicability due to the lack of the satellites visibility. In fact, due to this, an embedded Indoor Messaging System (IMES), based on a GPS receiver [4], has been proposed. It has the goal of seamless indoor-outdoor positioning providing better than GPS accuracies in indoor environments. Moreover, several alternative indoor positioning systems and techniques have been developed. In particular, embedded positioning systems based on Wi-Fi signals and fingerprinting techniques [5] are a common solution. Low positioning performance and high effort database building and maintenance, attribute to this solution a decreasing attention by the scientific community. Systems based on ultrasound sensors offer centimeter level positioning accuracy performance [6], however they are short range and highly affected by non-line-of-sight (NLOS) conditions. Nowadays, systems based on narrow-band radio frequency signals like Bluetooth Low Energy (BLE) [7] are becoming more and more popular. They are built using standard hardware and require low power consumption and low cost. The main drawback is the positioning performance. In general, this class of positioning systems is based on proximity algorithms and received-signal-strength (RSS) measurements, that are affected by multipath phenomena and lead to large positioning errors. In order to improve the performance, a high number of nodes may be required, increasing installation and maintenance costs. Systems based on Ultra Wide Bandwidth (UWB) signals are easily found in the literature [8]. They are characterized by fine resolution time measurements and better penetration properties with respect to the narrow-band solutions. However, obstructions in the direct path, that are common in crowded environments, contribute to the performance degradation. On the other hand, inertial navigation [9] and magnetic field based [10]-[13] positioning systems are not affected or are more resistant to NLOS conditions, respectively. Due to their integrative nature, inertial navigation systems are affected by rapidly growing positioning errors. Instead, magnetic fields based positioning systems usually rely on bulky and expensive electronic instruments and require high power consumption or are characterized by high complexity and computation. Specifically, the magnetic positioning system described in [12], based on three square-shaped low-frequency magnetic transmitters with side dimension of 1 m, and a three axis magnetic receiver, provides 2D and 3D position measurements. The obtained mean positioning error over an experiment area of approximately 30 m × 40 m, is 0.8 m and 0.4 m in the case of 3D and 2D positioning, respectively. The required current consumption for each transmitter is of the order of 7–8 A, and the analog to digital conversion at the receiver has a resolution of 24 bit. The outdoor remote positioning system in [13], which is based on magnetoquasistatic fields, provides 6 DoF measurements of a mobile transmitter by using seven magnetic field receivers. The magnetic transmitter with diameter of 16.5 cm is fed by a class E oscillator with a total output power of 0.56 W and the received signal by each receiver with diameter of 1 m is sampled with a resolution of 16 bit. The system performance is investigated over an outdoor experiment area of 27.43 m × 27.43 m with a mean positioning error of 0.77 m, mean inclination orientation of 9.67° and mean azimuthal orientation error of 2.84°.

In this paper, the authors investigate the performance of a first stage towards an embedded solution of a previously developed magnetic positioning system prototype [10][11], which showed a mean positioning error lower than 0.3 m over an indoor area of 12 m × 15 m and outdoor area of 14 m × 30 m. The required power and current consumption of each transmitter with radius equal to 14 cm is lower than 0.15 W

and 0.02 A respectively. Here, low cost microcontroller based boards have been used instead of high cost electronic instruments improving system portability and decreasing power consumption and cost. A positioning accuracy of the order of tens of centimeters is obtained over an area of approximately 50 m^2. The paper is organized as follows. Section II describes the theoretical basis of the measurement model while Section III provides an overview of the architecture description. In Section IV the experimental results are provided and described and in Section V the conclusions are given.

II. Measurement Model

In order to realize an embedded system solution, usually simplicity and low power requirements may be of fundamental importance. Thus, taking the previous goals in account, the developed magnetic positioning system prototype [10][11] is based on a simple measurement model. In the following, a short summary of the theoretical basics is reported. First, an electromagnetic point of view is considered. The magnetic field generated by a circular coil assumed in the coordinate system origin, in the near field zone, can be modeled as a magnetic dipole [14]

$$\mathbf{B}(x,y,z,t) = \frac{\mu_0}{4\pi}\left[3\mathbf{n}(\mathbf{m}\cdot\mathbf{n})d^{-3} - \mathbf{m}\,d^{-3}\right]e^{-j\omega t} \qquad (1)$$

where μ_0 is the free space magnetic permeability, $\mathbf{n}$ is the observation versor, $\mathbf{m}$ is the coil's magnetic moment, d is the observation distance, ω is the operating frequency and t is the time. The magnetic moment $\mathbf{m}$ is orthogonal to the coil surface and has a module m equal to $m = NIS$, where N is the number of turns in the coil, I is the feeding current and S is the coil's surface. According to Faraday's law of induction, the time varying magnetic field will couple a sensor coil with the field generating coil, inducing a voltage in the former [10][14]. In the case that both sensor coil and field generating coil are oriented in the same way, see Fig. 1(a), the relation between the induced voltage and the distance between the coil's centers, in a bi-logarithmic scale, can be expressed as:

$$\log_{10} V = a - b \log_{10} d \qquad (2)$$

where a is a hardware-configuration dependent constant and b has a nominal value of 3. The interested user can refer to [10] for detailed descriptions. In indoor environments, due to the interaction between the magnetic field and the different objects, the slope of the model (2) can assume different values [10]. Thus, a preliminary system calibration phase, that can be obtained by induced voltage measurements at known distances followed by linear fitting, is required in order to improve system accuracy and robustness [10][11]. During operating conditions, using calibration parameters and induced voltage measurements, ranging can be obtained by inverting (2).

In order to obtain high operating ranges without high power consumption requirements, resonant coils may be used [11]. Considering an equivalent circuit point of view, as in Fig. 1(b), it can be shown that the induced voltage is given by:

$$V \propto V_0 k \sqrt{Q_1 Q_2} \qquad (3)$$

where V_0 is the feeding voltage, k is the coupling factor and Q_1 and Q_2 are the resonator quality factors given by $Q=\omega L/R$, with L and R representing resonator's inductance and resistance, respectively. Thus, using high-Q resonant coils increases the induced voltage at a given distance. Consequently, once the receiver sensitivity is fixed, the operating range can be increased by using high-Q resonators. This is analogue to the antenna gains in a telecommunication system. High-Q resonators can be obtained by increasing the operating frequency, however this will increase the interaction between magnetic fields and surrounding environment [15], decreasing the system robustness. Thus, a tradeoff must be considered. In the following, an operating frequency of approximately 25 kHz will be used, since it provides good robustness and operating ranges up to 30 m or 12 m in line of sight (LOS) and NLOS conditions respectively.

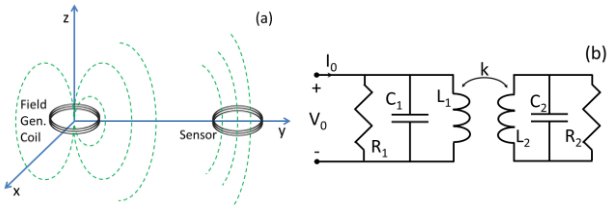

Fig. 1. Representation of the system configuration by considering an electromagnetic (a) and circuit (b) point of view. (a)-The magnetic field generated by a field generating coil at the coordinate system origin will couple with a sensor coil, inducing a voltage. Both the coils are assumed with the same orientation, lying in the *xy* plane. (b)-Circuit representation of the resonant coils assumption.

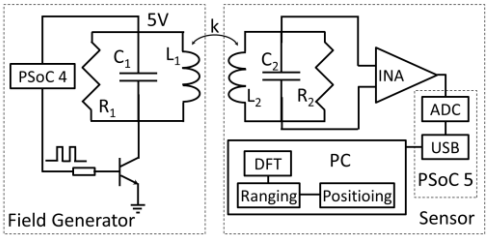

Fig. 2. Schematic of the system architecture. The field generating resonator is driven by a square wave signal provided by a PSoC 4 board. After being amplified by an INA, the output of the sensor coil is digitized by the PSoC 5 on-board ADC, and finally is transmitted through USB to a PC. Distance and position estimation are performed in the PC.

III. Architecture Description

The realized positioning system prototype is based on two types of system nodes, a set of magnetic field generating ones and a sensor node. A schematic representation of the system architecture, which is realized using off-the-shelf components, is shown in Fig. 2.

In particular, the field generating nodes are composed by a resonator and a driving circuit realized with a microcontroller based board, the Programmable System on Chip (PSoC) CY8CKIT-049 of the PSoC 4 family by Cypress. Each resonator is formed by the parallel connection between a circular coil with 20 turns of radius equal to 15 cm showing a nominal inductance of 128 µH and a lumped capacitor of 330 nF. The realized resonators have a nominal resonant frequency of 24.5 kHz and a quality factor of 12. The PSoC 4 board is programmed in order to provide a square wave signal with a frequency near to the resonance. Due to the resonator's band pass behavior, only the first harmonic of the square wave will have a significant contribution to the generated magnetic field, with the higher harmonics leading to a negligible effect. The required driving current has a maximum value of approximately 20 mA rms, leading to a magnetic field intensity

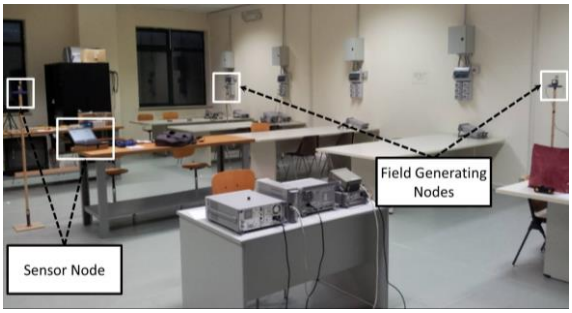

Fig. 3. Picture of the experiment environment. Two of the field generating nodes and the sensor node are shown.

of approximately one order of magnitude lower than the international regulations [10]. In order to avoid synchronization requirements that increase the system complexity, each field generating node is characterized by a particular frequency that is related with the known position of the node and identifies it at the receiver side.

The sensor node is composed by the same resonator as the field generating one, and also includes all the electronics for signal conditioning, acquisition and processing. Specifically, the induced voltage, which is self-filtered by the resonator, is first amplified by an instrumentation amplifier (INA), the integrated circuit AD8421BRZ by Analog Devices, and then acquired by a CY8CKIT-050 PSoC 5LP microcontroller based board. The digitalized signal, obtained by using a 12 bit ADC configured with a sampling rate equal to 75.65 kSa/s is transferred to a PC through a USB connection with the PSoC 5LP board. Then, the available signal, that comprises the contribution of all the field generating nodes plus noise, with a length of 30 kSa, after a flat-top windowing process, is used as an input to a DFT based algorithm for amplitude estimation. In particular, the usage of slightly different operating frequencies allows simultaneous amplitude estimation without time synchronization. Inverting the measurement model (2) and using the estimated amplitudes, range measurements are obtained. The Euclidean distance between a transmitting node with coordinates (x_i y_i) and the mobile node at a position with coordinates (x y) is given by $d_i = \sqrt{(x - x_i)^2 + (y - y_i)^2}$ while the corresponding estimated range is represented by $\hat{d}_i$. The measurement of the sensor node position relative to the field generating nodes is obtained by minimizing in a least squares sense the non-linear cost function given by:

$$E = \left[\hat{\boldsymbol{\Delta}} - \boldsymbol{\Delta}_{x,y}\right]^T \left[\hat{\boldsymbol{\Delta}} - \boldsymbol{\Delta}_{x,y}\right] \qquad (4)$$

where $\hat{\boldsymbol{\Delta}} = \left[\hat{d}_1 \;\; \hat{d}_2 \;\; \hat{d}_3 \;\; \hat{d}_4\right]^T$ contains the measured distances, $\boldsymbol{\Delta}_{x,y} = [d_1 \; d_2 \; d_3 \; d_4]$ contains the Euclidean distance between the field generating nodes and the position with coordinates (x y) and T is the transpose operator. Future developments include the realization of a fully embedded solution of the realized prototype. In particular, we are focusing on real time on-board amplitude estimation, range and position measurement without the usage of a PC.

IV. Experimental Results

In order to test the performance of the developed system prototype it was setup in a laboratory environment, as shown in Fig. 3, over an area of 7.2 m × 7.2 m. The system nodes were operating in LOS conditions, however several disturbing objects like metal cabinets, tables, chairs and electronic instruments were inside the experiment area. First, using four field generating nodes which do not require any time synchronization, static repeated measurements were performed in a set of nine known position points where real-time positioning of the sensor node was obtained. Then, position estimation in a dynamic scenario was considered. The results are shown in Figs. 4-6. In particular, in Fig. 4 the system deployment and the repeated measurement results are shown where the black squares represent the field generating node positions, the red diamonds the true positions and the blue asterisks the estimated positions. The measurement points were taken at the edges, at the center and at the side centers of a square with dimensions 3 m × 3 m. The true positions were manually surveyed with an estimated accuracy of the order of a couple of centimeters, and for each of them 150 position measurements were considered. The mean positioning error was evaluated for each point and a maximum value lower than 0.3 m was obtained. Further information regarding positioning error characteristics is provided by Fig. 5. In particular, the boxplot of the positioning error of all the considered points is shown. The positioning error shows a unimodal distribution and a maximum error of approximately 0.4 m, except a few outliers showing an error lower than 0.7 m. The mean error of all the measurements is approximately 0.17 m.

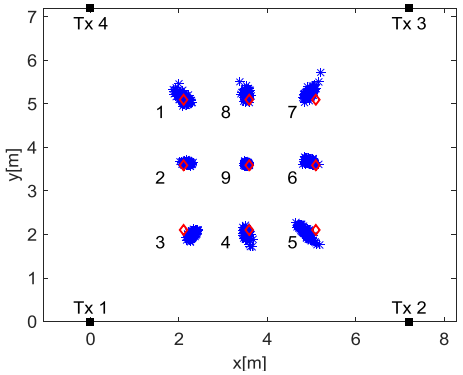

Fig. 4. Positioning results of 150 repeated measurements for each point over nine static points. The true positions are represented by the red diamonds while the estimated positions by the blue asterisks. Field generating resonator positions are shown by black squares.

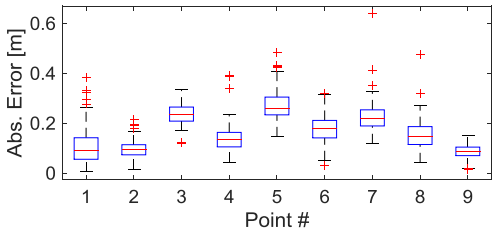

Fig. 5. Boxplot representation of the positioning error over the repeated measurements represented in Fig. 3. The central line of each box is the median error while the edges of each box represent the first and third quartile. Top and bottom ends of the dashed black lines are the maximum and minimum error with the red plus symbols representing outliers.

System simplicity, intended as measurement model leading to low computational cost, is obtained by using geometrical assumptions and limitations, such as operation in a planar and with equally oriented coils scenario. Since in general this can restrict the system applicability, measurements in a dynamic

scenario where the geometrical assumptions are not always satisfied are a key element for the system performance characterization. Two dynamic measurements were performed. In particular, a user followed a square reference path defined by the static measurement points, carrying the magnetic sensor node with himself. In both cases, the starting point was the number 1, shown by the black cross in Fig. 6. The first trajectory was the counterclockwise path starting in point 1 and ending in point 8, repeated three times. The second path was defined by two repetitions of the previous path, followed by the sequence 9-4-3-2-1-8-9. The real-time position estimation provided by the system is shown in Fig. 6. In particular, the blue dot-dashed line represents the first trajectory and the blue dashed line the second one. Estimated stop positions are represented by the magenta circle and the plus symbol. It can be clearly seen that the estimated positions are in good agreement with the followed paths. In general, it has been observed that misalignments or coplanarity deviations of the order of 10° only introduce a positioning error of the order of 5-10 cm [10][11]. System performance in outdoor scenarios was also tested, obtaining a similar performance even in larger coverage areas.

In general magnetic fields may be distorted by metals and/or different in-band noise sources in the environment. Some non-ideal effects, such as constant amplitude in-band interferences, can be mitigated by calibration, others may require lower operation frequency and/or higher SNR which can be obtained with higher power consumption. We have noted that the proposed method has a good robustness in typical indoor/outdoor environments since substantial part of the noise is filtered out by the band pass behavior of the resonators. Instead, in-band noise may be filtered out by considering non-linear coding and correlation techniques.

V. Conclusions

In this paper, a partially embedded version of a previously developed low cost magnetic positioning system is presented. A short overview of theoretical basics and system architecture is given and new obtained experimental results are discussed. Repeated measurements over an area of approximately 50 m^2 show a mean positioning error lower than 0.2 m with a maximum positioning error lower than 0.7 m. Moreover, measurements over two dynamic trajectories show good agreement with the reference path.

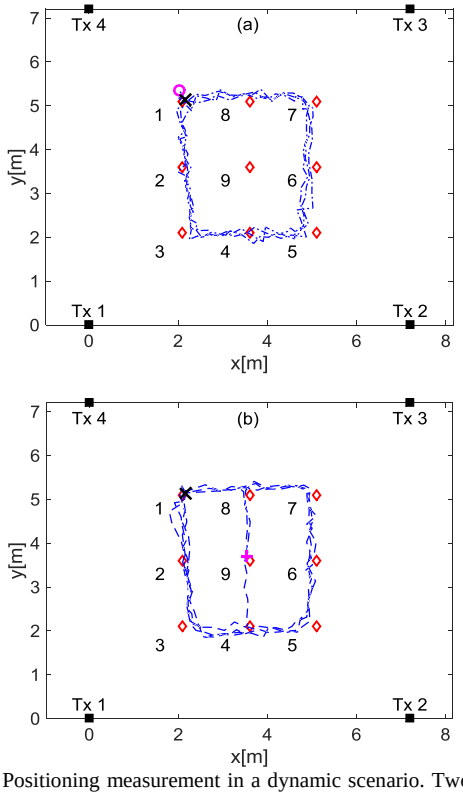

Fig. 6. Positioning measurement in a dynamic scenario. Two trajectories were followed with the first (a) consisting in the square defined by the external red diamonds and the second (b) consisting in two rectangles defined by the red diamonds. The results are represented by the blue dot-dashed line and the blue dashed line respectively. The start position is shown by the black cross and the stop positions by the magenta circle and magenta plus respectively.

References

[1] Perera, C.; Liu, C.H.; Jayawardena, S.; Min Chen, "A Survey on Internet of Things From Industrial Market Perspective," *IEEE Access*, vol.2, pp.1660-1679, 2014.

[2] Schiller, J., Voisard, A. "Location-based services," *Elsevier*, 2004.

[3] Barsocchi, P.; Chessa, S.; Furfari, F.; Potorti, F., "Evaluating Ambient Assisted Living Solutions: The Localization Competition," *IEEE Pervasive Comput.*, vol.12, no.4, pp.72-79, Oct.-Dec. 2013.

[4] IMES, [Online]. Available: http://gpsworld.com/wirelessindoor-positioningopening-up-indoors-11603/, May 2011.

[5] He, S.; Chan, S.-H.G., "Wi-Fi Fingerprint-based Indoor Positioning: Recent Advances and Comparisons," *IEEE Commun. Surveys Tuts., 2015.*

[6] De Angelis, A.; Moschitta, A.; Carbone, P.; Calderini, M.; Neri, S.; Borgna, R.; Peppucci, M., "Design and Characterization of a Portable Ultrasonic Indoor 3-D Positioning System," *IEEE Trans. Instrum. Meas.*, vol.64, no.10, pp.2616-2625, Oct. 2015.

[7] iBeacon, [Online]. Available: http://www.ibeacon.com/, Retrieved 2015.

[8] Conti, A.; Guerra, M.; Dardari, D.; Decarli, N.; Win, M.Z., "Network Experimentation for Cooperative Localization," *IEEE J. Sel. Areas Commun.*, vol.30, no.2, pp.467-475, February 2012.

[9] Nilsson, J. O.; Gupta, Amit K; Händel, P., "Foot-mounted inertial navigation made easy," *International Conference on Indoor Positioning and Indoor Navigation (IPIN), 2014*, pp.24-29, 27-30 Oct. 2014.

[10] Pasku, V., De Angelis, A., Dionigi, M., De Angelis, G., Moschitta, A., Carbone, P., "A Positioning System Based on Low Frequency Magnetic Fields," *IEEE Trans. Ind. Electron*, (**in press**), 2015.

[11] De Angelis, G., Pasku, V., De Angelis, A., Dionigi, M., Mongiardo, M., Moschitta, A., Carbone, P., "An Indoor AC Magnetic Positioning System," *IEEE Trans. Instrum. Meas.*, vol. 64, no. 5, pp. 1275-1283, May 2015.

[12] Sheinker A., Ginzburg B., Salomonski N., Frumkis L., and Kaplan B. Z., "Remote tracking of a magnetic receiver using low frequency beacons", *Measurement Science and Technology*, Vol. 25, 2014, 105101.

[13] Arumugam, D.D., Griffin, J.D., Stancil, D.D., Ricketts, D.S., "Three-Dimensional Position and Orientation Measurements using Magnetoquasistatic Fields and Complex Image Theory," *IEEE Antennas Propag. Mag.*, vol. 56, no. 1, pp. 160-173, Feb. 2014.

[14] Balanis, C. A., *Antenna theory: analysis and design*, Vol. 1, John Wiley & Sons, 2005.

[15] Pasku, V.; De Angelis, A.; Dionigi, M.; Moschitta, A.; De Angelis, G.; Carbone, P., "Analysis of the sensitivity of AC magnetic ranging systems to environmental configurations," *2015 IEEE International Instrumentation and Measurement Technology Conference (I2MTC)*, pp.1877-1882, 11-14 May 2015.